Advanced Energy Research Section

Sakhorn Rimjaem, Foreign Visiting Researcher
(Assistant Professor in Department of Physics and Materials Science, Faculty of Science, Chiang Mai University, 239, Huay Kaew Road, Muang District, Chiang Mai 50200, Thailand)

1. Summary

The author spent three months (Sep. 1, 2022-Nov. 30, 2022) as a guest associated professor at the Uji campus of Kyoto University, hosted by the Prof. H. Ohgaki's group.

Here the author reports about an investigation on study of solvation structure and dynamics of room-temperature ionic liquids using MIR free-electron laser.

2. Introduction

The unique set of properties of room-temperature ionic liquids (RTILs) has made them promising materials for modern electrochemical energy storage devices. One topic that has been under an intense debate is the free-charge carrier density in RTILs, which is one key to improving the efficiency of the devices. This quantity is strongly related to the short-range ion interactions and short-life interaction between ions and the surrounding molecules. Solvation structure, solvation dynamics, and hydrogen bond network are expected to be the key to a better understanding of such physical process, which is usually in the time scale of picosecond to femtosecond. Under the light of the MIR-FEL pump-probe (PP) experiment at KU FEL, the observation of interaction structure, interaction dynamics, and ion relaxation can be expected. Interpretation of experimental results can be done with the support from computational simulations.

3. Methodology

(1) Sample preparation

In this work we aimed to study the interaction lifetime and orientational decay of the ionic liquid 1-ethyl-3-methylimidazolium bis(trifluoromethylsulfonyl)imide ions ([Emim][NTf2]) when mixed with molecular solvent dimethyl sulfoxide (DMSO). In order to observe the effect of mixing ratio, [Emim][NTf2] (>98% HPLC, Merck KGaA) and DMSO (>99.9% anhydrous, Merck KGaA) were mixed to form binary mixtures with [Emim][NTf2] mole fraction XIL = 1.0, 0.9, 0.75, 0.5, 0.25, and 0.1 (the sample set includes sole DMSO, XIL = 0). Both chemicals were used as purchased and the samples were quickly prepared in ambient laboratory environment. The mixtures were kept in tightly closed glass vials and only few hundred μL of liquid sample was taken using a micropipette for each experiment. The sample was sandwiched between two diamond windows of an IR liquid cell with PTFE spacers for pathlength control. The pathlength was varied between 50 – 250 μm to obtain optimized signal.

(2) MIR-FEL pump-probe spectroscopy optical design and setup

The polarization selective PP setup was designed as shown in Figure 1. The FEL enters the setup and divided by a ZnSe beam splitter (BS) to form a pump beam and a probe beam. The pump beam is guided by the flat mirrors (M1 & M2) and is focused on the sample by a an off-axis parabolic mirror (OAP1). The probe beam is delayed by the optical delay line composed of two flat mirrors in retroreflector (RR) configuration. The computerized translational stage is used for optical path difference adjustment, which is in the range of 3 – 90 mm, to cover the required time delay of 10 – 300 ps. The probe beam is then reflected by the mirror (M3) and is focused by the OAP1 to spatially overlap with the pump beam in the sample volume. The transmitted pump beam is focused by OAP2 on the pyroelectric detector to collect as a pump-probe signal. The crossing angle between pump and probe beams at the sample is in the range of 10° – 20°. Two linear wire-grid polarizers are added for setting the polarization of the pump beam (P1) and for detecting the probe polarization (P2). The polarization angle of the probe beam can be switched between +45° and – 45° w.r.t. the probe polarization. Then, the ray optics simulation was carried out to determine all the required optical elements. The simulation was done based on the cloud-based software (3DOptix). An example of the ray simulation result and the 3D drawing of this setup made with a software FreeCAD are shown in Figure 2.

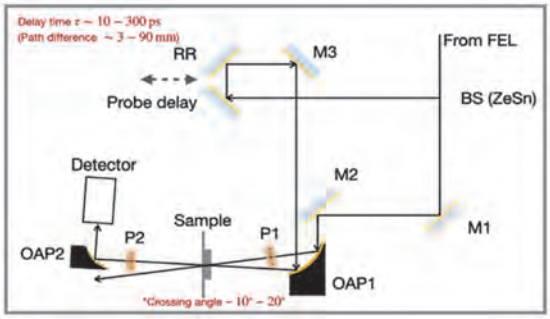

Fig. 1, Schematic design of the MIR-FEL polarization selective PP spectroscopy setup.

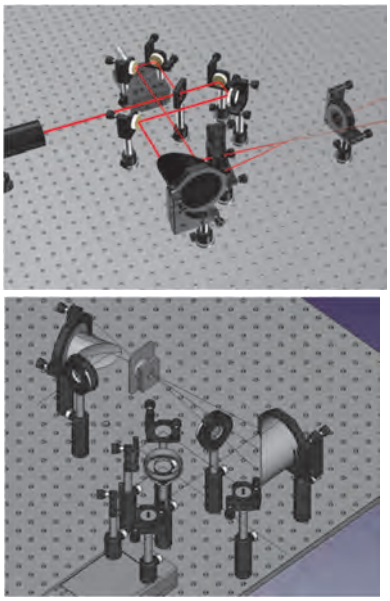

Fig. 2, (Top) A ray optics simulation to determine the specification of all optical elements. (Bottom) The 3D view of the designed setup.

The actual experimental setup at KU-FEL was set based on this drawing. The specifications of the key elements are OAP1 (90o, 3-in dim., 9-in. EFL), OAP2 (90o, 1-in dim., 2-in. EFL), flat mirrors (1-in dim.), and the crossing angle is 16^{o}.

4. Results and Discussion

The samples were first studied with FTIR spectroscopy to observe the absorption regions. The spectra show relatively much higher absorption on the fingerprint region (500 – 1500 cm^{-1}) than on the others. All absorption peaks look similar for all mixture samples and exhibit the combination of the [Emim][NTf2] and DMSO characters. The absorption of some [Emim][NTf2] peaks decrease with the mole fraction at wavenumber ~3160 cm^{-1}, which is the C–H stretches of the imidazolium ring alkyl or alkyl side chains. This shift is more pronounced when more DMSO is added. The shift indicates the existence of interaction between added solvent molecules and the cations. By using polarization selective PP spectroscopy with the FEL wavelength tuned to this vibrational mode at KU-FEL, we expect to be able to measure the lifetime of such interaction and probably the orientational decay of the ions.

The KU-FEL generated IR lasers at fundamental wavelength centered at ~6 μm (5.8 – 6.3 μm bandwidth). To obtain the desired wavenumber of ~3160 cm^{-1}, the second-harmonic generation (SHG) was applied by passing the FEL through the SHG crystal, which yielded the wavelength of ~3 μm (2.9 – 3.1 μm bandwidth). This wavelength corresponds to the required wavenumber of 3460 – 3185 cm-^{1}. The pump pulse energy was measured to be around 0.2 μJ prior the liquid cell. The pump-probe signal was measured by detecting the probe signal in comparison with the pump signal at varied optical delay path. We began the measurement with the pure [Emim][NTf2] at ~3160 cm^{-1} absorption line and there was no decay signal observed. We suspected the absorption at this wavelength is too low as shown by the IR spectrum. Therefore, we decided to try the measurement at higher IR absorption wavelength of ~1200 cm^{-1}. At this wavenumber the pump-probe signal also could not be detected but we observed the gas bubble formation in the sample liquid bulk, which is the indication of thermal dissipation as laser beam heated up the sample. We then tried to measure the response at ~1200 cm^{-1} in the mixture sample with XIL = 0.5, with the hope that the effect of strong absorption will be reduced to some level. Unfortunately, the expected exponential decay of the pump-probe intensity still could not be observed. Our postulate is the change in the probe signal is low since the population of the sample in the low vibrational state is low due to the excitation of the pump pulse.

With the FEL repetition rate of about 2856 MHz, the time between the consecutive pulse is about 0.3 ns. This is much shorter than the thermalization time of the liquid sample, meaning that the sample does not have enough time to relax. This issue has also been pointed out by [Novelli et al., PCCP, 2022]. They applied the THz FEL polarization selective pump-probe spectroscopy to study the dynamics of water with the setup similar to ours. For water having thickness of 50 μm, the thermalization time can be estimated to be in the order of 20 ms. With this in mind, the technique to modify the laser pulse train to have lower repetition rate is needed. Optical technique like plasma mirror is one option to allow ultrafast and high intensity beam to be selectively reflected. With such development, the pump-probe spectroscopy based on MIR-FEL light source may be achievable.

4. Conclusion

The experimental study to investigate the dynamics of ion interaction in ionic liquid/solvent mixtures using MIR-FEL polarization selective PP spectroscopy has been proposed. The work includes design and construction of the optical setup in pump-probe configuration. This setup alignment was carried out at KU-FEL to fit the beamline end station and used in the measurement. There was no observable pump-probe signal detected in any of the sample. This difficulty is attributed to the low absorption of the sample at the interested vibrational mode and too high repetition rate of the MIR-FEL. However, there was a positive indication showing that the designed setup is actually functioning. It seems from the current findings that additional optical technique may be required in the future to perform such experiment using the MIR-FEL.

[1]. Novelli F. et al 2022 *Phys. Chem. Chem. Phys.* 24 653

Advanced Energy Research Section

Josefine H.E. Proll, Foreign Visiting Researcher
(Assistant Professor at Eindhoven University of
Technology, Eindhoven, The Netherlands)

1. Summary

The author spent three months (Jan 01 2023 -Mar. 31, 2023) as a guest professor at the Uji campus of Kyoto University, hosted by the Heliotron J group.

Here the author reports about successes in turbulence modelling for Heliotron J.

2. Introduction

Recent successes in stellarator optimisation have allowed for the construction of neoclassically optimised stellarators such as Wendelstein 7-X and HSX. Experiments have shown [1,2] that the now dominant transport channel is turbulence. Thanks to the large space of available 3D magnetic field shapes, optimising also for turbulence is a possibility and might allow for stellarator and heliotrons configurations to be serious candidates for a DEMO reactor. Especially electrostatic turbulence driven at the ion scale, i.e. ion-temperature-gradient modes (ITG) and trapped-electron modes (TEM), have been found to significantly contribute to turbulent transport and have thus been studied in analytical theory and simulations in stellarator geometry. In so-called maximum-J configurations, of which W7-X is an approximation, it was shown analytically [3] that the classical electron-driven TEM was absent, which was shown to lead to low levels of turbulent heat flux (see Figure **2**) [4].

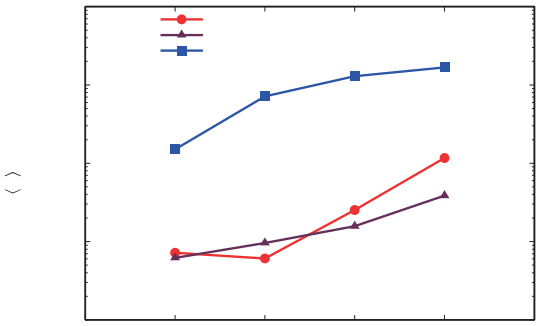

Figure 2: Normalised heat flux Q for grad-n-driven turbulence for different configurations. a/Ln is the density gradient scale length.

While HSX, a quasi-symmetric configuration and decidedly non-maximum-J, does not benefit from reduced linear growth rates (see Figure **1**), it does boast a similarly low turbulent heat flux. This unexpected nonlinear stabilisation has been attributed to the very low global shear of HSX and the subsequent increasedpool of subdominant and stable eigenmodes,

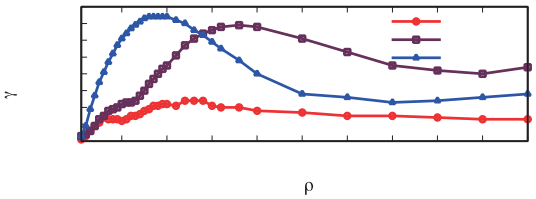

Figure 1: Linear growth rates of TEMs driven by a density gradient of a/Ln=3 in different configurations

to which energy can be transferred to reach saturation.

The question now is whether a configuration like Heliotron J, which is also approaching maximum-J-ness (albeit to a lesser degree than the high-mirror configuration of W7-X studied previously), and also has very low shear almost as low as HSX, can benefit from both mechanisms – the reduction of TEM thanks to maximum-J *and* improved saturation thanks to the low shear, and boast even lower heat fluxes. This would be a very interesting avenue to pursue for optimisation, as fully maximum-J configurations can be hard to achieve, especially over the full plasma radius. As an additional consequence of the absence of classical TEMs in W7-X, other types of modes can arise. Very recently, the so-called universal instability [5] has been identified in simulations in W-X geometry [6] and has been linked to potentially lower heat fluxes. Also in Heliotron J, the universal instability is expected to appear thanks to the postulated reduction of TEMs. During the research stay, several of these questions were addressed.

3. Gyrokinetic simulations for Heliotron J

To investigate whether the universal instability (UI) is indeed found in the different configurations of Heliotron J, linear simulations using the GENE code [7] were performed. Because the universal instability is predominantly driven by a density gradient, the temperature gradients of both ions and electrons were set to zero, and only a normalised density gradient of $a/L_n=3$ (with a being the minor radius and L_n the density gradient scale length) was chosen. Interestingly, in all configurations investigated, the universal instability is found to be dominant over a large range of low wave numbers (see Figure **4**), indicating that, similar to the case in Wendelstein 7-X, the UI might dominate the nonlinear transport and showcase enhanced saturation properties. Whether this is indeed the case is currently being investigated with nonlinear simulations. It is

remarkable that the UI is seen in ALL configurations of Heliotron J. In the ultra-high-bumpiness case ("5 to 0" in Figure **4** and Figure **3**) or the high-bumpiness case ("5 to 1"), the stability of the classical TEM and the subsequent emergence of the UI is somewhat expected, because these two configurations are approaching quasi-isodynamicity the most, whereas the standard configuration ("5 to 2") and the low-bumpiness configuration ("5 to 3") are less quasi-

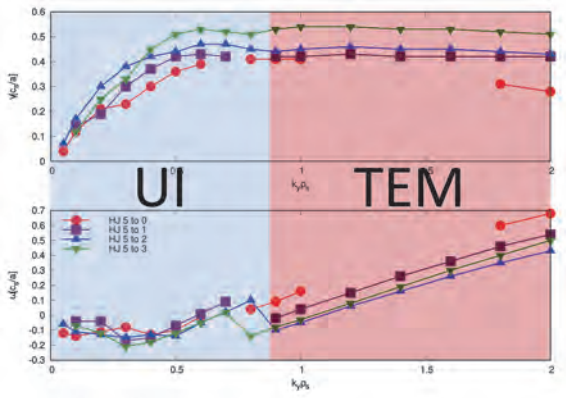

Figure 4: Linear growth rates of TEMs driven by a density gradient of a/Ln=3 in different configurations of Heliotron J, from low bumpiness (5 to 3) to ultra-high bumpiness (5 to 0)

isodynamic. However, it seems that even the lower degree of quasi-isodynamicity in the standard configuration and the low-bumpiness configuration is sufficient to stabilise the TEM. The theoretically predicted trend of higher degree of quasi-isodynamicity leading to lower TEM growth rates is seen regardless. These simulations are for pure density gradient with vanishing temperature gradients, which is very far from what is observed experimentally. To also perform computationally demanding nonlinear simulations (especially those with an electron-temperature-gradient require a lot of computing resources because the electron-scales need to be resolved, too), a joint proposal for computing time at IFERC was written between J. Proll and A. Ishizawa. The entire computing time asked for was granted, so that these investigations can continue full force in the coming months.

4. Available energy as a metric for turbulence

While the simulations above did show that a higher degree of quasi-isodynamicity (through a higher degree of bumpiness) leads to lower growth rates, we would need a nonlinear measure to assess whether also the actual levels of turbulence are reduced. To this end we can use the novel metric of available energy [8–10], a fully nonlinear expression which adheres to energy conservation and which has been shown to correlate remarkably well with the electron heat flux caused by trapped-electron modes. In our investigations, it was found (Figure **3**) that the available energy is generally reduced the higher the bumpiness is. While the available energy in its current form [10] is only that of the trapped electrons, and it is questionable that it would also faithfully represent turbulence driven by the passing-electron-driven UI, the results agree well with the linear results from the

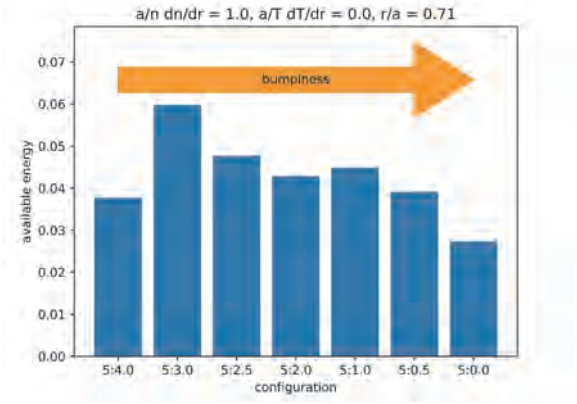

Figure 3: Available energy calculated for the different configurations of Heliotron J for a density gradient a/Ln=3.

previous section, and predict that the higher the bumpiness, the lower the turbulence. This would also explain the experimental findings where a higher bumpiness reported better overall confinement. A publication which compares the experimental results and the simulations and available energy calculations is in preparation. Moreover, work has begun to use the available energy as a metric to find turbulence-optimised configurations in the configuration space of Heliotron J, which might be used in one of the upcoming experimental campaigns.

6. Summary

We have confirmed that turbulence driven by TEMs is generally weak in Heliotron J and that higher bumpiness leads to enhanced stabilisation. Also the universal instability was found, as expected due to the high degree of quasi-isodynamicity. Work confirming the findings with nonlinear simulations is under way.

[1] C. D. Beidler et al., Nature **596**, 221 (2021).
[2] J. M. Canik et al., Phys Rev Lett **98**, 1 (2007).
[3] J. H. E. Proll et al., Phys. Rev. Lett. **108**, 245002 (2012).
[4] J. H. E. Proll et al., J. Plasma Phys. **88**, 905880112 (2022).
[5] P. Helander et al., Phys. Plasmas **22**, 090706 (2015).
[6] P. Costello et al., (2023).
[7] F. Jenko et al., Phys Plasmas **7**, 1904 (2000).
[8] P. Helander, J. Plasma Phys. **83**, (2017).
[9] P. Helander, J. Plasma Phys. **86**, 905860201 (2020).
[10] R. J. J. Mackenbach et al., Phys. Rev. Lett. **128**, 175001 (2022).